# Dynamical robustness of coupled heterogeneous oscillators

Gouhei Tanaka,[1,2,4] Kai Morino,[2] Hiroaki Daido,[3] and Kazuyuki Aihara[1,2,4]
[1]*Graduate School of Engineering, The University of Tokyo, Tokyo 113-8656, Japan*
[2]*Graduate School of Information Science and Technology, The University of Tokyo, Tokyo 113-8656, Japan*
[3]*Graduate School of Engineering, Osaka Prefecture University, Sakai 599-8531, Japan*
[4]*Institute of Industrial Science, The University of Tokyo, Tokyo 153-8505, Japan*
(Received 3 September 2013; revised manuscript received 1 April 2014; published 12 May 2014)

We study tolerance of dynamic behavior in networks of coupled heterogeneous oscillators to deterioration of the individual oscillator components. As the deterioration proceeds with reduction in dynamic behavior of the oscillators, an order parameter evaluating the level of global oscillation decreases and then vanishes at a certain critical point. We present a method to analytically derive a general formula for this critical point and an approximate formula for the order parameter in the vicinity of the critical point in networks of coupled Stuart-Landau oscillators. Using the critical point as a measure for dynamical robustness of oscillator networks, we show that the more heterogeneous the oscillator components are, the more robust the oscillatory behavior of the network is to the component deterioration. This property is confirmed also in networks of Morris-Lecar neuron models coupled through electrical synapses. Our approach could provide a useful framework for theoretically understanding the role of population heterogeneity in robustness of biological networks.

DOI: 10.1103/PhysRevE.89.052906 PACS number(s): 05.45.Xt, 89.75.Fb

## I. INTRODUCTION

Living systems are able to maintain their regular functions despite external and internal perturbations. In this sense, robustness is one of the fundamental characteristics of biological systems [1,2]. On the other hand, biological systems that have evolved to be tolerant to specific perturbations are often extremely fragile to other types of perturbations [3]. Exploration of the trade-off between robustness and fragility in complex biological systems is essential for understanding diseases and considering effective treatments from the viewpoint of systems biology. However, a mathematical framework for analyzing biological robustness has yet to be fully established [4].

Inspired by oscillation phenomena widely observed in biological systems [5,6], Daido and Nakanishi [7] presented a mathematical framework to examine robustness of coupled oscillator networks. Suppose that initially all the oscillator components are active, or showing self-sustained oscillation. When a fraction $p$ of the oscillators are inactivated, or changed to damped oscillators, due to aging or damage, the average oscillatory activity over the whole network is decreased. At a critical fraction $p = p_c$, the global oscillatory state turns to a nonoscillatory quiescent state. This phenomenon is called an aging transition [7]. The critical fraction $p_c$ has been examined for various types of networks, including globally coupled networks [7–10], locally coupled networks [11], multilayered networks [12], and complex networks [13,14]. Since a larger value of $p_c$ implies that the global oscillation is more tolerant to inactivation of the oscillators, $p_c$ can be used as a measure for evaluating dynamical robustness of oscillator networks [7]. Based on this measure of dynamical robustness, it has been demonstrated that the property of dynamical robustness can be different from that of structural robustness in complex networks [13]. The dynamical robustness measure has also been used to argue an efficient recovery of oscillation in damaged oscillator networks [15]. In almost all the above studies, the coupled oscillator systems consist of two subpopulations: the group of identical active oscillators and that of identical inactive oscillators.

In actual biological networks, however, biological components are not identical but heterogeneous in their activities and responses. There is significant variability in oscillation frequencies and amplitudes among individual biological oscillators: neurons in the suprachiasmatic nucleus, which produce synchronized oscillation relevant to circadian rhythms, display cell-to-cell variability in their oscillatory behavior [16,17]; protein regulatory circuits show wide fluctuations in oscillation amplitudes among individual cells [18]; neuronal oscillators in cortical networks exhibit diverse rhythmic patterns [19].

Here, we study the effect of population heterogeneity on the dynamical robustness of oscillator networks. Population heterogeneity is represented by a distribution of the control parameter, corresponding to the potential ability to oscillate, in the individual oscillator model. In this context, there have been a few studies on globally coupled networks [20,21]. We deal with more general networks of coupled heterogeneous oscillators and examine how tolerant the global oscillatory behavior is to continuous reduction in the control parameters, representing deterioration of the individual oscillators. As the average of the control parameters decreases, an order parameter evaluating the level of global oscillation diminishes. When the average of the control parameters falls below a critical value, the global oscillation vanishes. We analytically derive a general formula for this critical point and obtain an approximate formula for the order parameter near the critical point in networks of coupled Stuart-Landau oscillators. Our theoretical analysis can be applied to oscillator networks with various network topologies and parameter distributions representing component heterogeneity. Using the critical point as a measure for dynamical robustness of oscillator networks, we show that heterogeneity of oscillator components enhances the network's tolerance to the component deterioration. Furthermore, we demonstrate that this property is observed in

 

networks of Morris-Lecar neuron models coupled through electrical synapses.

## II. ANALYSIS AND RESULTS

### A. Coupled oscillator models

A network of $N$ diffusively coupled heterogeneous oscillators is described as follows [13]:

$$\frac{dz_j}{dt} = (\alpha_j + i\Omega - |z_j|^2)z_j + \frac{K}{N}\sum_{l=1}^{N} A_{jl}(z_l - z_j), \quad \text{for } j = 1,\ldots,N, \tag{1}$$

where $z_j$ $(=x_j + iy_j)$ is the complex variable of the $j$th oscillator, $\alpha_j$ is the real parameter controlling the potential activity of the $j$th oscillator, $\Omega$ is the natural frequency, and $K$ is the coupling strength. The dynamics of single isolated oscillators is represented by the Stuart-Landau oscillator [22]: $dz_j/dt = (\alpha_j + i\Omega - |z_j|^2)z_j$. This equation corresponds to a normal form of the supercritical Hopf bifurcation, which is a typical mechanism for the onset of oscillation in dynamical systems [5,6,22,23]: for $\alpha_j > 0$, the isolated oscillator exhibits a stable limit-cycle motion with amplitude $\sqrt{\alpha_j}$ and frequency $\Omega$; for $\alpha_j < 0$, the state converges to a stable equilibrium after transient damping oscillation. Note that $|\alpha_j|$ controls the strength of attraction to the stable state. The connectivity of the oscillators is represented by the adjacency matrix $A = (A_{jl})$, where $A_{jl} = A_{lj} = 1$ if the $j$th and $l$th oscillators are coupled and $A_{jl} = A_{lj} = 0$ otherwise. The degree of the $j$th oscillator node is denoted by $k_j \equiv \sum_{l=1}^{N} A_{jl}$ and the mean degree by $\langle k\rangle = (1/N)\sum_{j=1}^{N} k_j$.

Figure 1 illustrates a network with random topology [24], consisting of $N(=32)$ coupled heterogeneous oscillators. For $j = 1,\ldots,N$, the parameter $\alpha_j$ in Eq. (1) controls the behavior of the $j$th oscillator when it is isolated: if $\alpha_j > 0$, the oscillator facilitates the global oscillation in the network; otherwise, it suppresses the global oscillation. The facilitation or suppression is more effective for a larger value of $|\alpha_j|$. We assume a distribution of $\alpha_j$ $(j = 1,\ldots,N)$ to introduce population heterogeneity. The level of global oscillation is measured by the order parameter $|Z|$ where $Z = \sum_{j=1}^{N} z_j/N$. The deterioration of the individual oscillators is represented by a continuous decrease in $\alpha_j$ for all $j$, which is simply characterized by a decrease in the average value $\mu = \sum_{j=1}^{N} \alpha_j/N$. When $\alpha_j$ is positive for all $j$ as in Fig. 1(a), the global oscillatory behavior is observed. After a decrease in $\mu$, the global oscillation can be still maintained but the oscillation amplitudes are relatively small as shown in Fig. 1(b). A further decrease in $\mu$ causes a loss of sustained oscillation as shown in Fig. 1(c). Therefore, as $\mu$ continuously decreases, the oscillator network is expected to exhibit a transition from a global oscillatory state to a nonoscillatory state at a critical point $\mu = \mu_c$. Our aim is to analytically derive this critical value and clarify the impact of population heterogeneity on dynamical robustness of coupled oscillator networks.

### B. Derivation of the critical point

We derive the condition for the critical point at which the global oscillation vanishes, using the heterogeneous mean-field approximation [25]. We assume that a network consists of $M$ subpopulations of oscillators, in each of which the control parameters are identical. Namely, we set $\alpha_j = a_m$ for $j \in S_m$ $(m = 1,\ldots,M)$ where $S_m$ denotes the set of indices of the oscillators included in the $m$th subpopulation. The proportion of the oscillators in the $m$th subpopulation is denoted by $p_m$, satisfying $\sum_{m=1}^{M} p_m = 1$. For sufficiently large $N$, the number of the oscillators belonging to the $m$th subpopulation in the neighbors of the $j$th oscillator is expected to be $k_j p_m$. Therefore, the sum of the inputs to the $j$th oscillator in Eq. (1)

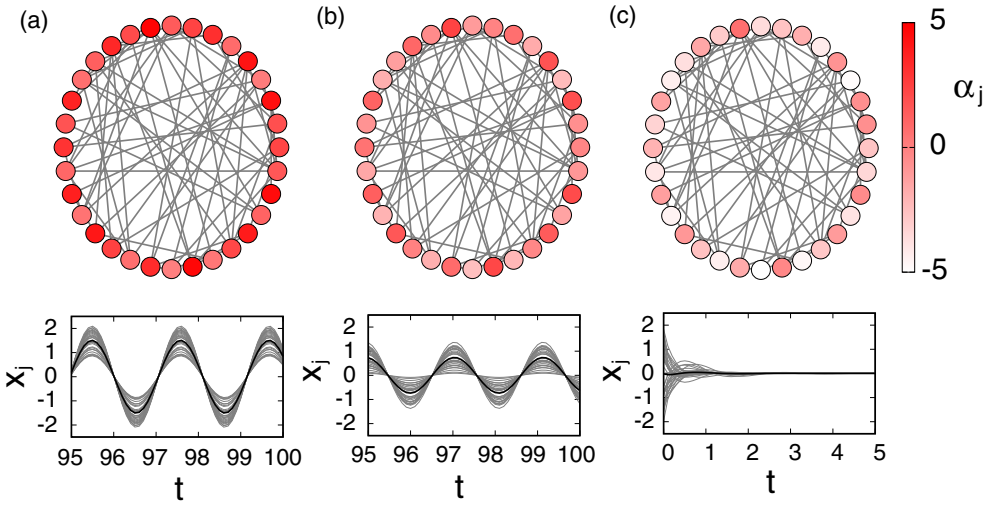


FIG. 1. (Color online) The upper panels illustrate random networks of coupled heterogeneous oscillators. The model equation is given by Eq. (1), where $N = 32$, $\Omega = 3$, $K = 10$, and $\langle k\rangle = 4$. The color intensity corresponds to the value of $\alpha_j$, indicating the activity of the oscillator when it is isolated. The value of $\alpha_j$ was randomly chosen from $[\mu - 5/2, \mu + 5/2]$: (a) $\mu = 5/2$; (b) $\mu = 0$; (c) $\mu = -5/2$. The lower panels show the time evolutions of the real parts $x_j$ of all the state variables (the gray lines) and the ensemble average (the black line).

is approximated as follows:

$$\sum_{l=1}^{N} A_{jl} z_l \simeq k_j \sum_{m=1}^{M} p_m H_m(t), \tag{2}$$

where the mean field for each subpopulation is given by

$$H_m(t) \equiv \frac{\sum_{j\in S_m} k_j z_j(t)}{\sum_{j\in S_m} k_j} \quad \text{for} \quad m = 1,\ldots,M. \tag{3}$$

The above approximation means that the oscillators with the same degree in the same subpopulation are regarded to behave identically. As shown in Fig. 1, numerical observations suggest that all the oscillators are synchronized in phase. Therefore, the state variables can be written as $z_j(t) = r_j(t)\exp[i(\Omega t + \theta)]$, where $r_j$ is the amplitude and $\theta$ is the phase delay. The mean fields are rewritten as follows:

$$H_m(t) = R_m(t) e^{i(\Omega t+\theta)} \quad \text{for} \quad m = 1,\ldots,M, \tag{4}$$

where $R_m(t) = [\sum_{j\in S_m} k_j r_j(t)]/(\sum_{j\in S_m} k_j)$. By using Eqs. (2) and (4), Eq. (1) can be reduced to the following equation for the oscillation amplitude:

$$\frac{dr_j}{dt} = \left(\alpha_j - \frac{Kk_j}{N} - r_j^2\right) r_j + \frac{Kk_j}{N} \sum_{m=1}^{M} p_m R_m. \tag{5}$$

The stationary amplitude $r_j^*$ is obtained by solving the equilibrium condition $dr_j/dt = 0$, that is,

$$r_j^3 - \left(\alpha_j - \frac{Kk_j}{N}\right) r_j - \frac{Kk_j}{N} \sum_{m=1}^{M} p_m R_m = 0. \tag{6}$$

Under the assumption $\beta_j \equiv \alpha_j - Kk_j/N < 0$ for all $j$, the equation above has a positive solution given as follows:

$$r_j^* = \left(\frac{\gamma_j}{2} + \sqrt{\left(\frac{\gamma_j}{2}\right)^2 - \left(\frac{\beta_j}{3}\right)^3}\right)^{1/3} + \left(\frac{\gamma_j}{2} - \sqrt{\left(\frac{\gamma_j}{2}\right)^2 - \left(\frac{\beta_j}{3}\right)^3}\right)^{1/3}, \tag{7}$$

where $\gamma_j \equiv (Kk_j/N)\sum_{m=1}^{M} p_m R_m$.

The self-consistency condition for the mean-field amplitudes $R_m$ $(m = 1,\ldots,M)$ is given by

$$R_m = G_m(R_1,\ldots,R_M) \quad \text{for} \quad m = 1,\ldots,M, \tag{8}$$

where

$$G_m(R_1,\ldots,R_M) \equiv \frac{\sum_{j\in S_m} k_j r_j^*(R_1,\ldots,R_M)}{\sum_{j\in S_m} k_j}. \tag{9}$$

A solution with $R_j > 0$ for all $j$ corresponds to a global oscillatory state, whereas the solution with $R_j = 0$ for all $j$ to a nonoscillatory quiescent state. Hence, the critical point is characterized by using the following matrix:

$$J = \left[\begin{array}{ccc} \frac{\partial G_1}{\partial R_1} & \cdots & \frac{\partial G_1}{\partial R_M} \\ \vdots & \ddots & \vdots \\ \frac{\partial G_M}{\partial R_1} & \cdots & \frac{\partial G_M}{\partial R_M} \end{array}\right]\Bigg|_{R_1=\cdots=R_M=0}. \tag{10}$$

From Eqs. (7) and (9), the $(m,n)$ entry of $J$ is evaluated as

$$\left.\frac{\partial G_m}{\partial R_n}\right|_{R_1=\cdots=R_M=0} \simeq \frac{p_n}{p_m d}\left(\frac{1}{N}\sum_{j\in S_m} \frac{d_j^2}{d_j - \alpha_j/K}\right), \tag{11}$$

where $d_j \equiv k_j/N$ is the degree normalized by the system size and $d \equiv \sum_{j=1}^{N} d_j/N$ corresponds to the link density for large $N$. From the assumption $\beta_j < 0$ for all $j$, the above formula requires the condition $d_{\min} - a_{\max}/K > 0$, where $d_{\min}$ denotes the minimum normalized degree and $a_{\max}$ the maximum value of $a_m$ for $m = 1,\ldots,M$. Moreover, the term inside the parentheses in the right-hand side of Eq. (11) is approximated as $p_m F(a_m)$ with

$$F(\alpha) \equiv \frac{1}{N}\sum_{j=1}^{N} \frac{d_j^2}{d_j - \alpha/K} = \sum_k P(k) \frac{(k/N)^2}{k/N - \alpha/K}, \tag{12}$$

where $P(k)$ denotes the degree distribution. Accordingly, the matrix $J$ is expressed as follows:

$$J = \frac{1}{d}\left[\begin{array}{ccc} p_1 F(a_1) & \cdots & p_M F(a_1) \\ \vdots & \ddots & \vdots \\ p_1 F(a_M) & \cdots & p_M F(a_M) \end{array}\right]. \tag{13}$$

The condition that one of the eigenvalues of $J$ is unity yields the following formula for the critical point:

$$\sum_{m=1}^{M} p_m F(a_m) - d = 0. \tag{14}$$

This result indicates that the critical value depends on the interplay among the network topology, the dynamical properties of the individual oscillators, and the size of the subpopulations.

Equation (14) for a network composed of multiple subpopulations includes the results of the previous studies on two subpopulations (i.e., two groups of active and inactive oscillators) as special cases. By setting $M = 2$, $p_1 = 1 - p$, $p_2 = p$, $a_1 = a > 0$, and $a_2 = -b < 0$ and solving Eq. (14) with respect to $p$, we can derive the critical point for the globally coupled network with $d_j \simeq 1$ as $p_c = a(K + b)/[(a + b)K]$ [7] and that for more complex networks as $p_c = [F(a) - d]/[F(a) - F(-b)]$ [13].

Now, let us examine the effect of population heterogeneity on the critical threshold in the oscillator networks where the control parameter values are continuously distributed. For a given range $[a_{\min}, a_{\max}]$ of the control parameter values, we set $a_m = a_{\min} + \frac{m-1}{M-1}(a_{\max} - a_{\min})$ for $m = 1,2,\ldots,M$. Further, the proportion of the subpopulation size $p_m$ is assumed to follow a distribution with probability density function $h(a_m)$. For analytical tractability, we consider the case that the degree $k_j$ and the parameter $\alpha_j$ are uncorrelated.

When the network structure is a random graph [24] and the parameter $\alpha_j$ is uniformly distributed in $[\mu - \delta/2, \mu + \delta/2]$, it follows that $F(\alpha) \simeq d^2/(d - \alpha/K)$ and $h(\alpha) \simeq 1/\delta$. In the thermodynamic limit $N \to \infty$ and the continuous limit

$M \to \infty$, the condition (14) yields

$$\int_{\mu-\delta/2}^{\mu+\delta/2} \frac{1}{\delta} \frac{d^2}{d-\alpha/K} d\alpha - d = 0. \tag{15}$$

By solving this equation, we obtain the critical value $\mu_c$ as follows:

$$\mu_c = Kd + \frac{\delta}{2} \frac{e^{-\delta/(Kd)}+1}{e^{-\delta/(Kd)}-1}. \tag{16}$$

In the strong-coupling limit $K \to \infty$, $\mu_c$ approaches 0 which is the bifurcation point of the single isolated oscillator [20]. In the weak coupling limit $K \to 0$, $\mu_c$ approaches $-\delta/2$.

Similarly, we can formally describe a conditional equation satisfied by the critical point for any other networks where the degree distribution is given by $P(k)$ and the probability density function of the parameter distribution is given by $h(\alpha)$. However, it is not generally possible to get an explicit expression of $\mu_c$ due to the difficulty in the integral calculation.

### C. Analysis of the order parameter

We analyze the order parameter in the vicinity of the critical point. When the oscillators are synchronized in phase, the order parameter $|Z|$ is equivalent to $R \equiv \sum_{m=1}^{M} p_m R_m$. From $\gamma_j = (Kk_j/N)R$, the stationary amplitude $r_j^*$ in Eq. (7) is written as $r_j^* = \hat{r}_j^*(R)$. Therefore, using Eqs. (8) and (9), the self-consistency condition for the order parameter $R$ is written as follows:

$$R = \sum_{m=1}^{M} p_m \frac{\sum_{j\in S_m} k_j \hat{r}_j^*(R)}{\sum_{j\in S_m} k_j} \simeq \frac{1}{dN^2} \sum_{j=1}^{N} k_j \hat{r}_j^*(R), \tag{17}$$

where the approximation $\sum_{j\in S_m} k_j \simeq p_m dN^2$ is used. Expanding $\hat{r}_j^*$ with respect to $R$ around $R = 0$ as

$$\hat{r}_j^*(R) = \sum_n \frac{1}{n!} \frac{\partial^n \hat{r}_j^*(0)}{\partial R^n} R^n, \tag{18}$$

we obtain

$$R = \left[ \frac{1}{dN} \sum_{j=1}^{N} \frac{d_j^2}{d_j - \alpha_j/K} \right] R - \left[ \frac{1}{KdN} \sum_{j=1}^{N} \left( \frac{d_j}{d_j - \alpha_j/K} \right)^4 \right] R^3 + O(R^4). \tag{19}$$

Note that the coefficient of the first order term in the right-hand side of the above equation is equivalent to $(1/d)F(\alpha)$. Once the normalized degree $d_j (= k_j/N)$ and the control parameter $\alpha_j$ are given for $j = 1, \ldots, N$, the order parameter can be numerically calculated by solving Eq. (19) with respect to $R$ after neglecting the fourth and higher order terms.

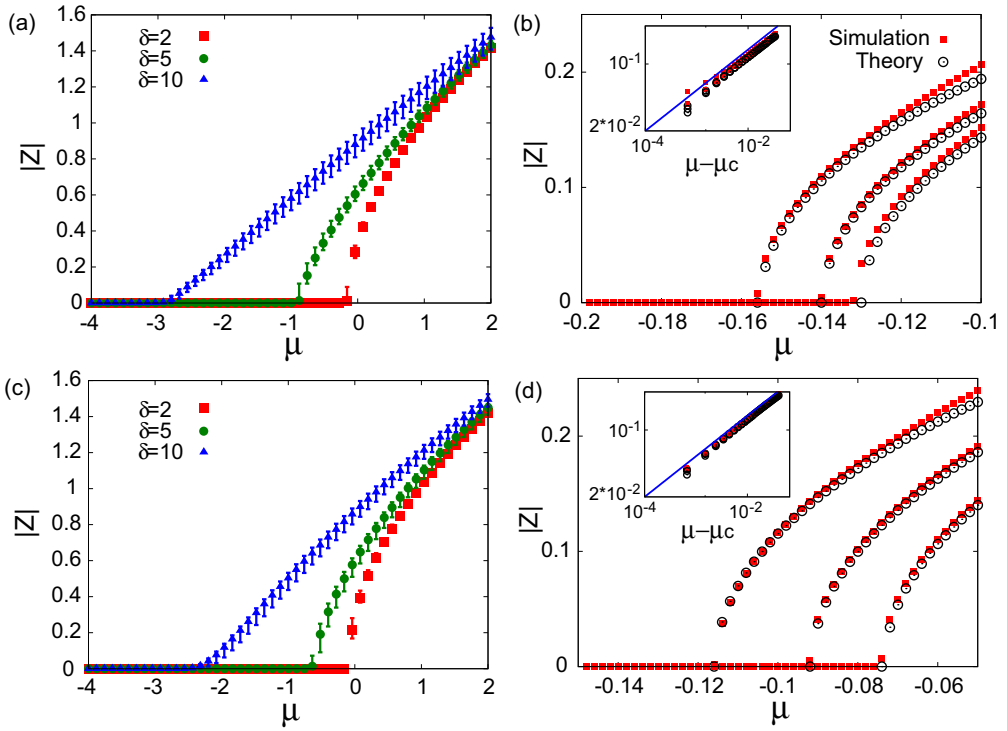


FIG. 2. (Color online) The order parameter $|Z|$ is plotted against the average $\mu$ under the uniform distribution of $\alpha_j$ in Eq. (1), where $N = 1000$, $\Omega = 3$, $K = 10$, $d \sim \langle k \rangle/N = 0.08$, and $\alpha_j \in [\mu - \delta/2, \mu + \delta/2]$. (a) Results for random networks. Each plot is the average of ten simulations and the error bar indicates the maximum and minimum values. (b) Comparison between the theoretical and numerical values of the order parameter for three sample random networks with $\delta = 2$. The inset is a log-log plot of the order parameter near the critical point for all the three samples. The blue solid line with slope 1/2 shows a scaling property. (c) The same as (a), but for scale-free networks. (d) The same as (b), but for three sample scale-free networks with $\delta = 2$.

### D. Numerical simulations

We validate the analytical results with numerical simulations. The fourth-order Runge-Kutta method with time step 0.1 is used for numerical integration of the model and the initial conditions are randomly set to be $z_j(0) \in [-1,1]$ for $j = 1,\ldots,N$. The macroscopic oscillation level of the entire network is evaluated by the order parameter $|Z|$. Figure 2(a) demonstrates the variations of the order parameter with a change in the average control parameter $\mu$ for three different cases of population heterogeneity $\delta$ in random networks. A breakdown of the oscillator network occurs at a critical value of $\mu$ in each case, which is smaller for a larger value of $\delta$. Figure 2(b) shows that the theoretical prediction of the order parameter obtained from Eq. (19) is in good agreement with the numerical results for three sample networks with $\delta = 2$. The inset shows the scaling property of the order parameter near the critical point, i.e., $|Z| \propto (\mu - \mu_c)^{\lambda}$, where the critical exponent $\lambda$ is estimated as $1/2$. However, for $\delta = 10$, the value of the exponent seems to be different from $1/2$ as shown in Fig. 2(a), probably due to the strong population heterogeneity. Note that the formula (19) is not valid in this case because the condition $d_{\min} - a_{\max}/K > 0$ is not satisfied. Figures 2(c) and 2(d) are the results for the oscillator networks with scale-free structure. The effect of the population heterogeneity $\delta$ on the critical $\mu$ value in these networks is similar to that in the random networks. In comparison between Figs. 2(a) and 2(c), we observe that the critical $\mu$ value for a random network is smaller than that for a scale-free network when the population heterogeneity is the same. This property is also checked for $\delta = 2$ by comparing Figs. 2(b) with 2(d) (note that the scale of the horizontal axis is different). The validity of the approximate formula for the order parameter in Eq. (19) is confirmed for the scale-free networks as shown in Fig. 2(d). The scaling property of the order parameter for the scale-free networks is the same as that in the random networks.

Figure 3 shows that the theoretical values of the critical point obtained from Eq. (16) are in good agreement with the numerical results. In the numerical simulations, the parameter $\mu$ is decreased from a sufficiently large value for each $\delta$ and the transition is considered to have occurred if $|Z| < 10^{-6}$ at $t = 50\,000$. From Eq. (16), $\mu_c$ is a monotonically decreasing function of $\delta$. Namely, the heterogeneity of the oscillators enhances the network robustness to the deterioration of the oscillator components. We can also see that oscillator networks are more robust for more sparse networks as shown in Fig. 3(a) as well as for more weakly coupled networks as shown in Fig. 3(b). This is because the component deterioration has little negative impact on the global oscillatory behavior in such networks. In return for this merit, they are less likely to achieve globally synchronized oscillation.

To check the generality of our main result about the effect of population heterogeneity, numerical simulations were performed to compute the critical values for oscillator networks with combinations of different coupling schemes uniform coupling or weighted coupling), different network structures (random graph [24] or scale-free network [26]), and different distributions of $\alpha_j$ (uniform or Gaussian). Figure 4(a) shows the results for the network model with uniform coupling in Eq. (1) where the same coupling strength is assigned to each link. In all the cases, an increase in the standard deviation $\sigma$ of the distribution of $\alpha_j$ results in the almost monotonic decrease in the critical value $\mu_c$. Next, we consider the following oscillator network model with weighted coupling [14]:

$$\frac{dz_j}{dt} = (\alpha_j + i\Omega - |z_j|^2)z_j + \frac{K}{k_j}\sum_{l=1}^{N} A_{jl}(z_l - z_j), \quad \text{for} \quad j = 1,\ldots,N, \tag{20}$$

where the coupling strength is weighted by the inverse of the degree. The analyses of the critical point and the order parameter for this model are performed similarly to those in Secs. II B and II C, respectively. It should be noted that, instead of Eq. (12), the function $F$ is given by $F(\alpha) = 1/(1 - \alpha/K)$ in this case. Therefore, the critical point is not influenced by the network topology. When the network structure is a random graph [24] and the parameter $\alpha_j$ is uniformly distributed in $[\mu - \delta/2, \mu + \delta/2]$, the critical value is given by

$$\mu_c = K + \frac{\delta}{2}\frac{e^{-\delta/K} + 1}{e^{-\delta/K} - 1}, \tag{21}$$

which is independent of the link density $d$ unlike Eq. (16) for the networks with uniform coupling. Figure 4(b) shows that

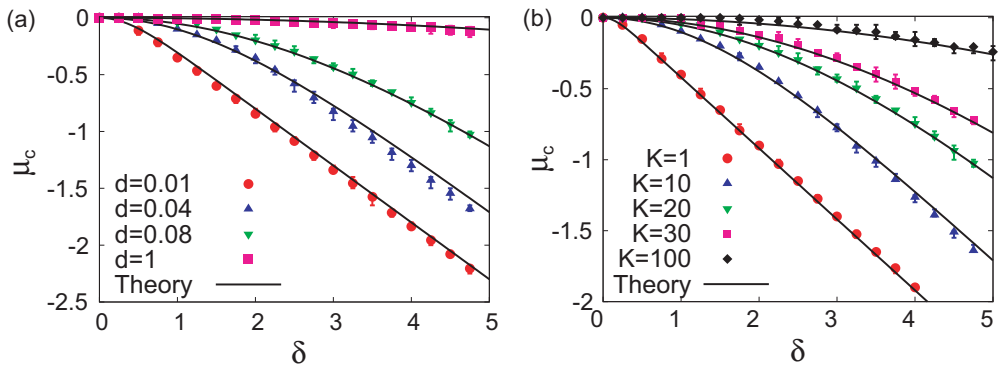


FIG. 3. (Color online) The critical value $\mu_c$ is plotted against the range $\delta$ of the uniform distribution of $\alpha_j$ in Eq. (1) with random topology, where $N = 3000$, $\Omega = 3$, and $\alpha_j \in [\mu - \delta/2, \mu + \delta/2]$. The symbols and solid curves indicate the numerically estimated values and the theoretical values obtained from Eq. (16), respectively. Each plot is the average of ten simulations and the error bar indicates the maximum and minimum values. (a) Results for different link densities. The coupling strength is fixed at $K = 10$. (b) Results for different coupling strengths. The link density is fixed at $d \sim \langle k \rangle / N = 0.08$.

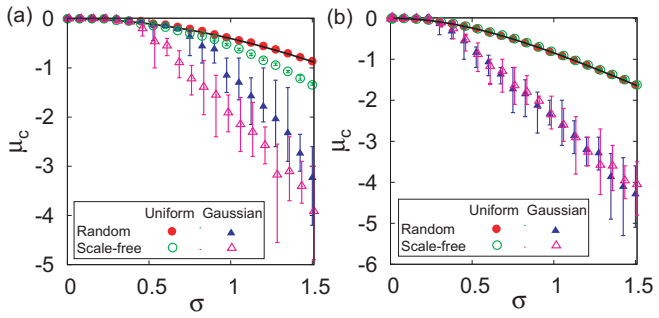


FIG. 4. (Color online) The critical value $\mu_c$ is plotted against the standard deviation $\sigma$ of the distribution of $\alpha_j$ in the networks where $N = 3000$, $\Omega = 3$, $K = 30$, and $d \sim \langle k \rangle / N = 0.08$. (a) Results for the network model with uniform coupling in Eq. (1). (b) Results for the network model with weighted coupling in Eq. (20). Each panel shows the four cases resulting from the combinations of the two factors: random or scale-free network topology; uniform or Gaussian distribution of the control parameter value $\alpha_j$, with mean $\mu$ and standard deviation $\sigma$. For the uniform distribution case, $\sigma = \delta/\sqrt{12}$. Each plot is the average of ten simulations and the error bar indicates the maximum and minimum values. The solid line represents the theoretical prediction, i.e., Eq. (16) for (a) and Eq. (21) for (b).

our main result is valid also for the oscillator network model (20) with weighted coupling.

### E. Coupled Morris-Lecar neuron models

Our framework is also useful to investigate the effect of population heterogeneity on dynamical robustness of coupled dynamical components exhibiting another type of bifurcation. We demonstrate numerical results for networks of coupled Morris-Lecar (ML) neuron models [27]. The ML neuron model exhibits repetitive spike firing when the external input current is increased beyond a certain threshold value. The mechanism for the onset of firing activity is a saddle-node on invariant circle (SNIC) bifurcation or a subcritical Hopf bifurcation, depending on the system parameter values [28]. The bifurcation type characterizes the dynamical property of the neuron model: the former type is called a class I neuron and the latter type a class II neuron [29]. The ML neuron model has been used in the studies on mixed populations of excitable and oscillatory units [8,21].

The networks of ML neuron models coupled via electrical synapses (gap junctions) are described as follows [30]:

$$C_{\mathrm{M}} \frac{dV_j}{dt} = I_j^{\mathrm{ext}} - I_j^{\mathrm{ion}} - I_j^{\mathrm{syn}}, \tag{22}$$

$$\frac{dW_j}{dt} = [W_\infty(V_j) - W_j]/\tau_W(V_j), \tag{23}$$

for $j = 1, \ldots, N$, where $V_j(t)$ represents the membrane potential, $W_j(t)$ represents the recovery variable, $W_\infty(V) = \{1 + \tanh[(V - V_3)/V_4]\}/2$, and $\tau_W(V) =$

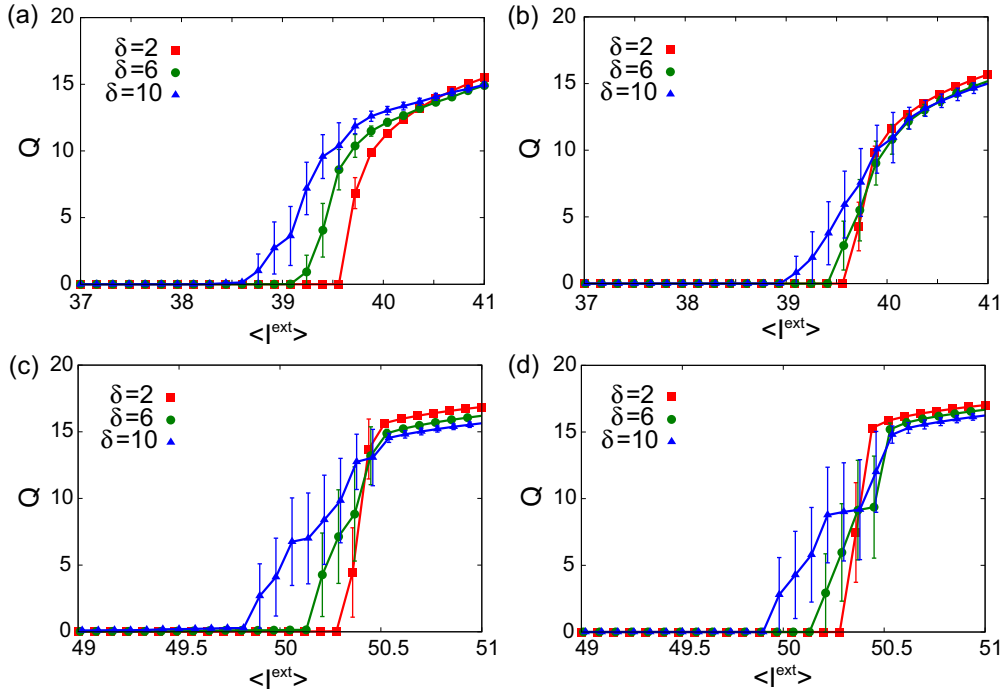


FIG. 5. (Color online) The order parameter $Q$ plotted against the mean external input $\langle I^{\mathrm{ext}} \rangle$ in the networks of Morris-Lecar neuron models coupled via electrical synapses, given by Eqs. (22) and (23). The number of neurons is set at $N = 200$ and the mean degree at $\langle k \rangle \sim 4$. The system parameter values are set at $C_{\mathrm{M}} = 20$, $g_{\mathrm{K}} = 8$, $g_{\mathrm{Ca}} = 4$, $g_{\mathrm{L}} = 2$, $V_{\mathrm{K}} = -80$, $V_{\mathrm{Ca}} = 120$, $V_{\mathrm{L}} = -60$, $V_1 = -1.2$, $V_2 = 18$, $V_4 = 17.4$, $\phi = 1/15$ [28], and $g_{\mathrm{gap}} = 1$ [30]. We set $V_3 = 12$ for class I neurons and $V_3 = 2$ for class II neurons [28]. The heterogeneity of the neurons is represented by $\delta$, which is the range of the uniform distribution of the external input. Each plot is the average over ten simulations and the error bar indicates the standard deviation. (a) Random networks of class I neurons. For an isolated class I neuron, a saddle-node on invariant circle bifurcation occurs at $I^{\mathrm{ext}} \sim 39.7$ (see Ref. [28] for details). (b) Scale-free networks of class I neurons. (c) Random networks of class II neurons. For an isolated class II neuron, a subcritical Hopf bifurcation occurs at $I^{\mathrm{ext}} \sim 50.4$ (see Ref. [28] for details). (d) Scale-free networks of class II neurons.

$1/\{\phi \cosh[(V - V_3)/(2V_4)]\}$. The ionic current $I_j^{\rm ion}$ is given by $I_j^{\rm ion} = g_{\rm L}(V_j - V_{\rm L}) + g_{\rm Ca}M_\infty(V_j)(V_j - V_{\rm Ca}) + g_{\rm K}W_j(V_j - V_{\rm K})$, where $M_\infty(V) = \{1 + \tanh[(V - V_1)/V_2]\}/2$. We set $V_3$ at different values for modeling class I and class II neurons while keeping the other parameters fixed [28]. The synaptic current $I_j^{\rm syn}$ through a gap junction is given by $I_j^{\rm syn} = \sum_{l=1}^{N} g_{jl}(V_j - V_l)$, where the coupling strength is $g_{jl} = g_{\rm gap}$ if neuron $j$ and neuron $l$ are connected and $g_{jl} = 0$ otherwise. The external input current $I_j^{\rm ext}$ is the control parameter for the individual neurons. Therefore, we assume that $I_j^{\rm ext}$ is uniformly distributed in the range $[\langle I^{\rm ext}\rangle - \delta/2, \langle I^{\rm ext}\rangle + \delta/2]$, where $\langle I^{\rm ext}\rangle$ is the mean external input current and $\delta$ represents the degree of heterogeneity of the neurons. The level of neuronal firing in the entire network is evaluated by the order parameter $Q = \sqrt{\langle |\mathbf{x}_c - \langle \mathbf{x}_c\rangle|^2\rangle}$, where $\mathbf{x}_c = (1/N)\sum_{j=1}^{N}(V_j(t), W_j(t))$ is the centroid and the brackets mean a long time average [7,31,32]. The fourth-order Runge-Kutta method with time step 0.05 is used for numerical integration of the model. We randomly set the initial conditions to be $V_j(0) \in [-40,40]$ and $W_j(0) \in [-1,1]$ for $j = 1, \ldots, N$. In numerical simulations, the parameter $\langle I^{\rm ext}\rangle$ is decreased from a sufficiently large value for a fixed value of $\delta$ and the transition is considered to have occurred if $Q < 10^{-6}$ at $t = 50\,000$.

Figure 5 shows the variation of the order parameter with a change in the mean external input current $\langle I^{\rm ext}\rangle$. As the mean external input current decreases and falls beyond a critical value, the neuronal firing in the whole network is lost in all the cases. In the networks consisting of class I neurons, the component heterogeneity enhances the robustness of the firing activity in both random and scale-free networks as shown in Figs. 5(a) and 5(b). The same effect of population heterogeneity is found in the random and scale-free networks of class II neurons as shown in Figs. 5(c) and 5(d).

## III. SUMMARY AND DISCUSSION

In the analysis of the Stuart-Landau oscillator networks, we have derived the general condition for the critical point at which a loss of global oscillation occurs as the individual oscillator components deteriorate. By comparing the critical values for networks with different levels of heterogeneity in the oscillator components, we have shown that the dynamical robustness of the oscillator networks is enhanced by the population heterogeneity. This property is considered to be widely observed in networks of dynamical components exhibiting a supercritical Hopf bifurcation, such as those widely found in chemical, biological, and engineering systems [5,6,22,23], because the Stuart-Landau oscillator is a normal form of the supercritical Hopf bifurcation. Moreover, we have obtained the approximate formula for the order parameter in the vicinity of the critical point and confirmed its validity with numerical simulations. In the simulations of coupled Morris-Lecar neuron models with different types of bifurcation phenomena, we have shown that the population heterogeneity makes the neuronal network more tolerant to component deterioration.

Our framework enables to analyze the transition between two different dynamical regimes in complex networks of dynamical components, each of which exhibits a bifurcation phenomenon. The critical point for the transition, as a measure of dynamical robustness, is normally affected by the network topology, the characteristics of the dynamical components, and the heterogeneity of the components. Nevertheless, the effect of population heterogeneity on the dynamical robustness is common to the models addressed in this paper. It is a future work to check this property in more biologically plausible models. The methods for identifying mathematical models of heterogeneous cell populations from experimental data [33] would be useful for theoretically understanding the role of heterogeneity in biological robustness.

## ACKNOWLEDGMENTS

This research was partially supported by JSPS KAKENHI Grants No. 24700222 (G.T.) and No. 22540397 (H.D.), as well as the Aihara Innovative Mathematical Modelling Project, the Japan Society for the Promotion of Science (JSPS) through the "Funding Program for World-Leading Innovative R&D on Science and Technology (FIRST Program)," initiated by the Council for Science and Technology Policy (CSTP) (G.T., K.M., and K.A.).

[1] A. L. Barabási and Z. N. Oltvai, Nat. Rev. Genet. **5**, 101 (2004).
[2] H. Kitano, Nat. Rev. Genet. **5**, 826 (2004).
[3] J. M. Carlson and J. Doyle, Proc. Natl. Acad. Sci. USA **99**, 2538 (2002).
[4] H. Kitano, Mol. Syst. Biol. **3**, 137 (2007).
[5] S. H. Strogatz, *Nonlinear Dynamics and Chaos* (Perseus, Cambridge, MA, 2000).
[6] A. T. Winfree, *The Geometry of Biological Time*, 2nd ed. (Springer, New York, 2001).
[7] H. Daido and K. Nakanishi, Phys. Rev. Lett. **93**, 104101 (2004).
[8] D. Pazó and E. Montbrió, Phys. Rev. E **73**, 055202(R) (2006).
[9] H. Daido and K. Nakanishi, Phys. Rev. E **75**, 056206 (2007).
[10] G. Tanaka, Y. Okada, and K. Aihara, Phys. Rev. E **82**, 035202(R) (2010).
[11] H. Daido, Europhys. Lett. **84**, 10002 (2008).
[12] K. Morino, G. Tanaka, and K. Aihara, Phys. Rev. E **83**, 056208 (2011).
[13] G. Tanaka, K. Morino, and K. Aihara, Sci. Rep. **2**, 232 (2012).
[14] Z. He, S. Liu, and M. Zhan, Physica A **392**, 4181 (2013).
[15] K. Morino, G. Tanaka, and K. Aihara, Phys. Rev. E **88**, 032909 (2013).
[16] S. Bernard, D. Gonze, B. Čajavec, H. Herzel, and A. Kramer, PLoS Comput. Biol. **3**, 0667 (2007).
[17] D. K. Welsh, J. S. Takahashi, and S. A. Kay, Annu. Rev. Physiol. **72**, 551 (2010).
[18] N. Geva-Zatorsky, N. Rosenfeld, S. Itzkovitz, R. Milo, A. Sigal, E. Dekel, T. Yarnitzky, Y. Liron, P. Polak, G. Lahav *et al.*, Mol. Syst. Biol. **2**, 2006.0033 (2006).

[19] G. Buzsáki and A. Draguhn, Science **304**, 1926 (2004).
[20] H. Daido, Phys. Rev. E **84**, 016215 (2011).
[21] H. Daido, A. Kasama, and K. Nishio, Phys. Rev. E **88**, 052907 (2013).
[22] Y. Kuramoto, *Chemical Oscillations, Waves, and Turbulence* (Springer-Verlag, Tokyo,1984).
[23] J. Guckenheimer and P. Holmes, *Nonlinear Oscillations, Dynamical Systems, and Bifurcations of Vector Fields* (Springer, Berlin, 1983).
[24] P. Erdős and A. Rényi, Publ. Math. Inst. Hung. Acad. Sci. **5**, 17 (1960).
[25] R. Pastor-Satorras and A. Vespignani, Phys. Rev. Lett. **86**, 3200 (2001).
[26] A. L. Barabási and R. Albert, Science **286**, 509 (1999).
[27] C. Morris and H. Lecar, Biophys. J. **35**, 193 (1981).
[28] K. Tsumoto, H. Kitajima, T. Yoshinaga, K. Aihara, and H. Kawakami, Neurocomp. **69**, 293 (2006).
[29] J. Rinzel and G. B. Ermentrout, in *Methods in Neuronal Modeling*, edited by C. Koch and I. Segev (MIT Press, Cambridge, MA, 1989), pp. 135–169.
[30] P. Balenzuela and J. Garciá-Ojalvo, Phys. Rev. E **72**, 021901 (2005).
[31] D. Golomb and J. Rinzel, Phys. Rev. E **48**, 4810 (1993).
[32] A. S. Pikovsky, M. G. Rosenblum, and J. Kurths, Europhys. Lett. **34**, 165 (1996).
[33] J. Hasenauer, S. Waldherr, M. Doszczak, N. Radde, P. Scheurich, and F. Allgöwer, BMC Bioinf. **12**, 125 (2011).